Peer-reviewed version available at Remote Sens. 2018, 10, 1369; doi:10.3390/rs10091369

Type of the Paper (Article)

On the Very High-Resolution Radar Image Statistics of the Exponential Correlated Rough Surface: Experimental and Numerical Studies

Ming Jin [1], Kun-Shan Chen [1]* and Dengfeng Xie [2]

[1] State Key Laboratory of Remote Sensing Science, Institute of Remote Sensing and Digital Earth, Chinese Academy of Science; jinming@radi.ac.cn
[2] University of Chinese Academy of Science; Xiedf@radi.ac.cn
* Correspondence: chenks@radi.ac.cn; Tel.: +86-010-6485-2531

Abstract: The aim of this study is to investigate, by means of experimental measurements and full-wave simulations, the dominant factors for the very high-resolution (VHR) radar image speckles from exponential correlated rough surfaces. A Ka-band radar system was used to collect the return signal from such a surface sample fabricated by 3D printing, and that signal was further processed into images at different resolution scales, where the image samples were obtained by horizontally turning around the surface sample. To cross-validate the results and to further discuss the VHR speckle properties, full wave simulations by full 3D Finite Difference Time Domain (FDTD) method were conducted with 1600 realizations for the speckle analysis. At the considered very high resolution, speckle statistics show divergence from the fully developed Rayleigh distribution. The factors that impact on the high-resolution speckle properties from exponential correlated rough surface, are analyzed in views of the equivalent number of scatterers theory and scattering scales, respectively. From the data results and extended discussions, it is evident that both of the above factors matter for VHR speckle of backscattering, from the exponential correlated rough surface as a good representative for the ground surface.

Keywords: SAR Speckle; Rough Surface Scattering; Exponential Correlation; Very High Resolution

1. Introduction

In the context of radar imagery, understanding the speckle properties is imperative for both image de-noising and applications such as land-cover classification and parameters retrieval [1-4]. Radar speckle arises due to the coherent sum of numerous distributed scattering contributions [3]. A general assumption is the "fully developed" speckle model, which is applicable when the resolution cell size is much larger than the correlation length (l) of the ground surface [3]. This requirement may be met in low-to-medium image resolution. The fully developed speckle model is based on the following two hypotheses: (1) total scattering is contributed by independent scatters; (2) there is a sufficiently large number of scatters contributing to a resolution cell so that a complex Gaussian distribution is followed. For VHR radar images, these assumptions are no longer valid. As a result, the K-distribution is often applied to model the speckles [5-6].

Speckle statistic variation with the resolution cell size or antenna footprint has been a subject of interest in rough surface scattering [7-12]. As the radar image resolution evolves from tens of meters to approximately 1 meter, or even a smaller size, this topic becomes more important currently for land observations. In order to model high resolution speckle properties, Di Martino et al, proposed the predicting method for the equivalent number of scatterers within the resolution cell [12], considering stochastic stationary rough surface description, and more advanced, fractal surface models. In this work, we address the topic of VHR radar speckle statistics using indoor SAR experiments and supporting full-wave simulations.

Since the prediction for the equivalent number of scatterers has been established in [12], it is used as an evaluating tool in this work. To be specific, the exponential correlated rough surface is considered, due to its rich high frequency roughness on the surface-air interface, which leads to numerous local scattering contributions. In particular, 3-D printing process was used to fabricate sample surface that is used for scattering measurement conducted at Ka band. In this manner, the image resolution scale close to the rough surface correlation length can be achieved, i.e., the image resolution cell size can be at the same scale of the surface geometric gurgitation. In this view, the scattering mechanism from exponential correlated rough surface is similar to that from sea surface, where small scale scattering process is modulated by large scale gurgitation [13]. The prediction for the equivalent number of scatterers per resolution cell from [12] is served as a reference in the analysis. Meanwhile, based on the results from experimental and supporting numerical practices considering different incident directions, the effects of scattering scale on the speckle properties can be observed. Further numerical studies are conducted with different RMS height, for discussions on both the factors of the equivalent number of scatterers, and the scattering scaling effects.

This work is similar to that reported in [11], but different. One of the differences is that the authors focus on the VHR radar speckles from the exponential correlated rough surface. Another difference is that numerical studies by 3D-FDTD simulations are included to support the data analysis as well as the discussions on the physical process. The remainder of this paper consists of 4 parts. In section II, the rough surface sample generation, the experimental and numerical methods, are demonstrated with verification results. In section III, the measured images, simulated backscattering, and their amplitude statistics are presented and analyzed. In section IV, with supporting numerical results, the VHR radar speckle properties are further discussed. Finally, the contribution of this work is highlighted in the conclusion.

2. Experimental and Numerical Methods

In this work, to study the VHR rough surface speckles, both the experiments and full-wave numerical simulations are conducted. In this section, the configurations and procedures are to be demonstrated.

2.1. The Rough Surface Samples

In this paper, an exponential correlation function for the random rough surface is used since it describes better for the natural surface [4]. For both the experimental target fabrication and numerical discretization, digital samples are generated. Specifically, the spectrum method is used to generate digital samples, that: by generating the roughness spectrum components with random phase and amplitude distribution following Eq. (1), then performing inverse Fourier transform, one obtains the digital sample. The geometric roughness parameters of the rough surface samples are listed in Table 1. In addition, the roughness spectrum of the exponential correlation surfaces is plotted in **Error! Reference source not found.**.

$$\mathrm{W}(k_\rho) = \frac{h^2 l^2}{2\pi}(1 + k_\rho^2 l^2)^{-\frac{3}{2}} \tag{1}$$

where h is surface *RMS* height, and l is correlation length.

In fact, it has been difficult to actually fabricate an exponential correlated experimental sample, due to the rich high frequency roughness. In this work, the 3D printing technique was utilized for the fabrication. This technique allows one to directly manufacture actual samples based on the computer-generated digital sample with designed parameters, as shown in Table 1. As should be noted, the considered sample has rich high frequency roughness, which generates numerous local scatters, leading to the strong speckle effects.

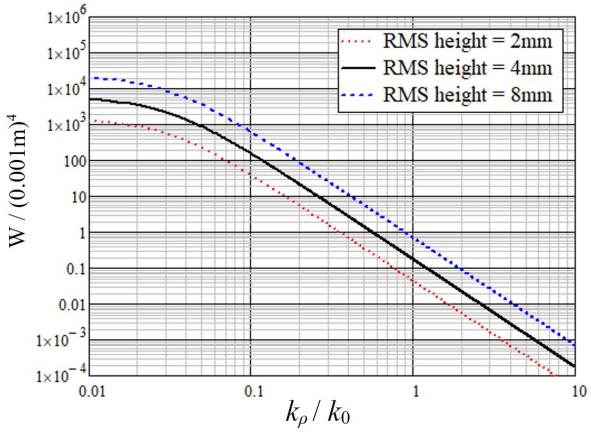

Figure 1. Surface roughness spectrum of the considered rough surface samples at 32 GHz ($k_0 = 2\pi/\lambda$). (Exponential correlated rough surface, correlation length l of 48mm)

Table 1. Parameters of the exponential correlated rough surface samples

	Size	*h*	*l*
Measured Sample	250 mm in diameter	4mm	48 mm
(in λ @ 32 GHz)	26.7 in diameter	0.427	5.12
Numerical Samples	125mm × 125mm	2mm,4mm,8mm,12mm	48 mm
(in λ @ 32 GHz)	13.3 × 13.3	0.214, 0.427, 0.854, 1.281	5.12

More specifically, the FDM (Fused Deposition Modeling) technique is utilized for the fabrication. In this 3D printing process very thin lines of fused materials are continuously printed to construct a structure, and a 100% filling rate can be achieved to form a solid. By this way the shaping accuracy of about 0.5mm can be achieved, which is approximately $\lambda/20$ in the Ka band and sufficient for the imaging study. The main advantage of this technique is that it permits the usage of lossy printing material, so as to generate samples simulating the half space rough surface scattering scenario, such as the moist soil ground. In this work, the measured permittivity is 6.22-*j*2.86 at 32GHz, and that value was used in the FDTD computations.

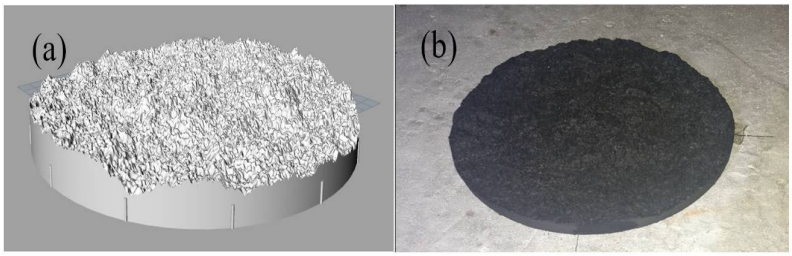

Figure. 1 Geometry Configuration of the 3D model and the fabricated sample of the exponential correlated rough surface. (a): CAD model; (b): Fabricated sample.

On the other hand, to obtain speckle results by numerical simulations, numerous digital samples are necessary to achieve a sufficiently large number of realizations [4]. In this work, the following procedures are excised: first a very large rough surface mesh is generated on grids, then the digital sample for each realization (400*400 meshing points) is cut from that large mesh. In the cutting, one sample is neighboring and overlapping to next with 100 discretize interval (100*interval size~31mm) distant, which is close to the footprint size in diameter in the numerical simulations. For the speckle study, 1600 (40*40) samples are obtained for one to achieve an enough number of realizations. The digital samples are then input into the FDTD simulator one by one for computing scattering in 3D computational domain.

2.2. Experimental Configuration and Procedure

The experimental imaging system is constructed based on a vector network analyzer (VNA) and a 1D scanner, as shown in Figure. 2. To achieve the rough surface imaging in the chamber, the measurements are performed in the Ka band. Detailed configuration parameters include as the following: the track span (L) is 800 mm with an interval of 8 mm; the distance between the target scene center and the antenna (T/R) is approximately 1400 mm; the transmitting and receiving antennas are of 20dBi gain with a half power beam angle of 17°. In the implementation, the height difference H and distance D can be varied accordingly to achieve the beam direction or incident direction angle θ_i of 30°, 40°, 50°, or 60°. The target is placed on a low-scattering supporting cylinder in the foam material, which is set on a motor driven rotation platform (for ϕ rotation as shown in Figure. 2). Multiple image acquisitions should be achieved for the speckle statistics. More specifically, in each case of θ_i, the imaging measurements for the rough surface sample are performed 20 times, and after each time ϕ is changed with an equal angular interval, as shown in Figure. 2. Therefore, 20 images are obtained for a specific θ_i, then speckle statistical analysis can be conducted based on those results.

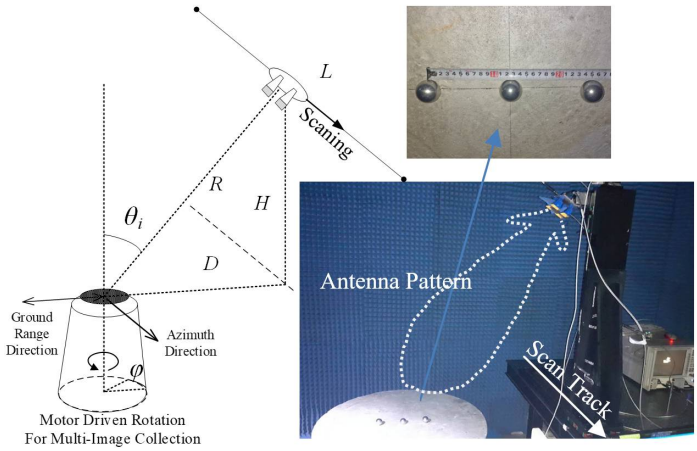

Figure. 2 Configuration of the indoor imaging measurement (sketch and photo). The 3 small spheres were utilized to compensate the antenna pattern effect.

In the scanning measurement, the scattering signals were captured through the antennas and VNA all along the scanning track and all over the Ka band. Then different bandwidths and synthetic aperture lengths were selected to achieve different spatial resolutions (in ground range), as concluded in Table 2. During the image processing, the Kaiser window (β=2.5) was utilized along the frequency and aperture signal. And the resolution cell size in Table 2 are realized in the presence of the Kaiser window.

Table 2. Imaging parameters for different resolution cell size (R=1.4 m, ground range resolution, Kaiser windows (β=2.5) applied in both domains).

Ground Resolution	*Center Frequency*	*Aperture Length*	*Bandwidth (GHz)*			
			θ_i: 30°	θ_i: 40°	θ_i: 50°	θ_i: 60°
30×30 mm²	32.0 GHz	240 mm	11.00	8.25	6.60	6.15
45×45 mm²		160 mm	7.35	5.50	4.40	4.10
60×60 mm²		120 mm	5.50	4.13	3.30	3.07
75×75 mm²		96 mm	4.40	3.30	2.65	2.45
90×90 mm²		80 mm	3.70	2.75	2.20	2.05

Peer-reviewed version available at Remote Sens. 2018, 10, 1369; doi:10.3390/rs10091369

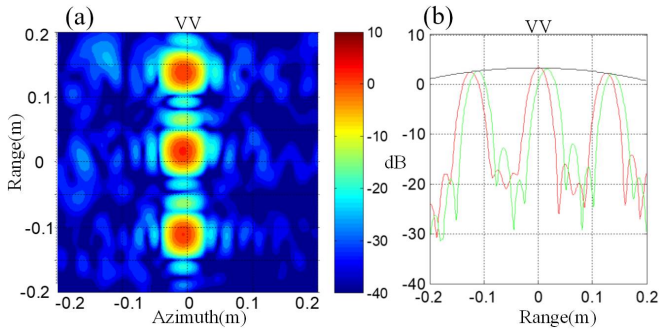

Figure. 3 Image and range profile of 3 small metal balls, showing the non-uniform illumination due to the antenna pattern effect. (a): Image; (b): Range profiles (The results in two cut lines are obtained by performing 180° rotation of φ in the measurements).

To calibrate the image amplitude results, one metal sphere of 30mm in diameter was used as the RCS reference. However, to study the speckle statistics of image amplitudes, ideally the rough surface sample should be uniformly illuminated by the transmitting antenna, and uniformly viewed by the receiving antenna. Unfortunately, the antenna patterns are not uniform on the measured sample, and their effects must be compensated, including both the transmitting and receiving antennas. In addition to the RCS calibration with one metal sphere and the range amplitude compensations commonly implemented in SAR processing, we further measured the images from a column of 3 metal balls in the ground range direction. Based on the image of these balls, the antenna pattern weighting was fitted along the range, and that fitting was then utilized to compensate the image amplitude, as shown in Figure. 2 and Figure. 3.

Finally, after the images from the rough surface were processed, calibrated, and compensated, the amplitude speckle results were obtained for the VHR radar speckle analysis.

2.3. Numerical Simulation Configuration and Procedure

Although the experimental study is the most straight-forward and reliable approach, it is restricted by the actual rough surface sample in both the aspects of number and size. On the other hand, the full-wave full-3D Finite Difference Time Domain (FDTD) simulator provides with complementary and extensible data support. This numerical method has been reported in computing scattering from homogenous and layered rough surfaces [14-15]. The FDTD simulator used in this work is developed based on that reported in [16] which is a full-3D simulator, and the scattering coefficients are obtained by averaging results from a large number of random numerical samples (realizations).

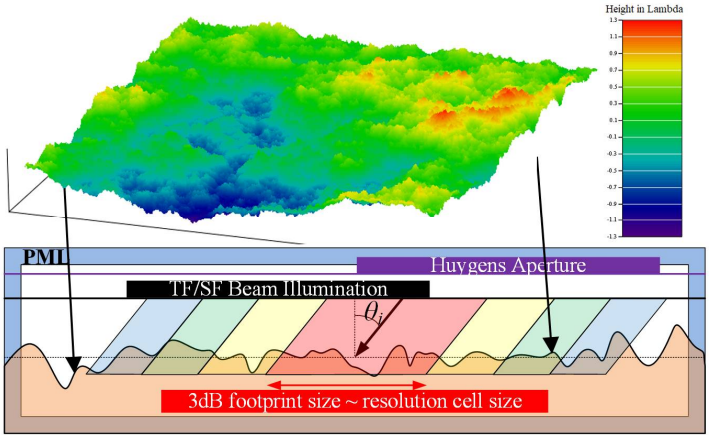

Figure. 4 Configuration of FDTD simulations for rough surface scattering

Figure. 4 shows the simulation configuration in each realization, which is a typical scene for the half-space scattering. In general, the tapered incident beam is injected by the Total Field/Scatter

Preprints (www.preprints.org) | NOT PEER-REVIEWED | Posted: 20 July 2018 doi:10.20944/preprints201807.0383.v1

Peer-reviewed version available at Remote Sens. 2018, 10, 1369; doi:10.3390/rs10091369

Field boundary (TF/SF), below that boundary the incident beam immerges to illuminate the rough surface, and above that the boundary scattered field can be extracted. The Huygens Aperture collects the recorded near-field scattered field and turns that into far-field results like scattering coefficients. On the other hand the Perfect Matching Layer (PML) is used to truncate the computation domain without introducing disturbing reflections.

In this work, a tapered wave with the fixed ground footprint is set for the illumination. In each realization, the incident beam is always pointing to the center of the rough surface. In this work, different incident angles θ_i are considered, namely, 30°, 40°, and 50°. Furthermore, cases of different surface *RMS* heights h are also considered to support the extended discussions. The discretization cell size in the FDTD simulation is set to 1/30λ at 32GHz, which is sufficient in modeling the high frequency roughness of the exponential correlated rough surface.

In general, the aim of this simulation work, which is similar to that reported in [4], is to investigate speckles by counting backscattering far-field amplitude results over a large number of realizations. The difference is that we focused on the VHR situation, that means we used a smaller tapered wave illumination region than those in the general rough surface scattering simulations. Specifically, the simulated resolution cell size is defined by the beam footprint in the numerical studies, realized by setting footprint size same to the required value (30 mm in a diameter for 3 dB edge power drop). The detailed computation parameters are summarized in Table 3, and these simulations are performed to support the conclusions drawn from the VHR radar imaging experiments with a 30 mm resolution as well as further discussions. In each realization, one separate rough surface sample is utilized to feed the FDTD simulator, and then, after all the realizations are completed, the speckle properties are concluded. The simulations were run on a 2-way Intel Xeon workstation with octal channel memories: one set of 1600 realizations required approximately 1 week, with each realization taking less than 5 min.

Table 3. Computational parameters for the FDTD simulations @ 32GHz.

Set 1	***3dB Footprint Size***	***ds***(mm)*	***Domain Size*(Yee cells⁺)**	***Realization number***	***θᵢ (h=4mm)***
	30mm in diameter	0.3123	400×400×180	1600	30°, 40°, 50°
Set 2	***3dB Footprint Size***	***ds***(mm)*	***Z Direction Size*(Yee cells)**	***Realization number***	***h*(mm) θᵢ=30°**
	30mm in diameter	0.3123	160, 180, 220, 280	1600	2,4,8,12

*Here, *ds* denotes the discretizing interval in the computation domain.

⁺Yee cell is the mesh cell in the FDTD

2.4. Verification Results

In this section, we present the verification results to validate the fabricated experimental sample and the utilized numerical simulator.

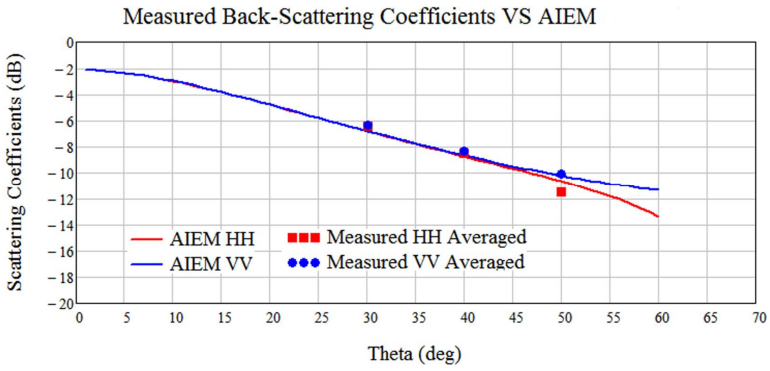

Figure. 5 Comparison between measured scattering coefficients (σ_0) of the exponential correlated rough surface sample, and the results by AIEM prediction, at 32 GHz.

First, to validate the fabricated sample for the experimental imaging tests, we directly measured its scattering coefficients without imaging process. Since in the scattering coefficient

measurement only one data sample can be obtained through one measurement, apparently more angular samples (in φ) are needed than those for the imaging measurement. Actually, more than 48 sets of backscattering data were obtained by the ϕ angle rotation in this case. The backscattering RCS data were obtained with the calibration by the metal sphere and then normalized into scattering coefficient, with the actual section of the rough surface sample. The measured scattering coefficients are compared with the AIEM model predictions [17,18] at different θ_i, clearly, good agreement can be observed.

Secondly, to validate the FDTD simulator, the computational domain was increased to 1200×1200×180 Yee cells in the domain size, so as to obtain converged scattering coefficients. In other words, the rough surface aperture size was increased to $40\lambda\times40\lambda$. It should be noted that, in common scattering simulations for rough surfaces [4], the aperture size of $32\lambda\times32\lambda$ can be regarded as sufficiently large. Because of the huge computational burden, with one realization requiring approximately 1 hours, only 50 realizations are performed to obtain the averaged scattering coefficients distributions over the upper space. Again, the AIEM results are utilized as reference, and two sets of results are compared in Figure. 6. Although the FDTD results failed in presenting a smooth contour due to the insufficiently large realization number, the results by numerical and analytical methods clearly agree well with each other in the distribution patterns.

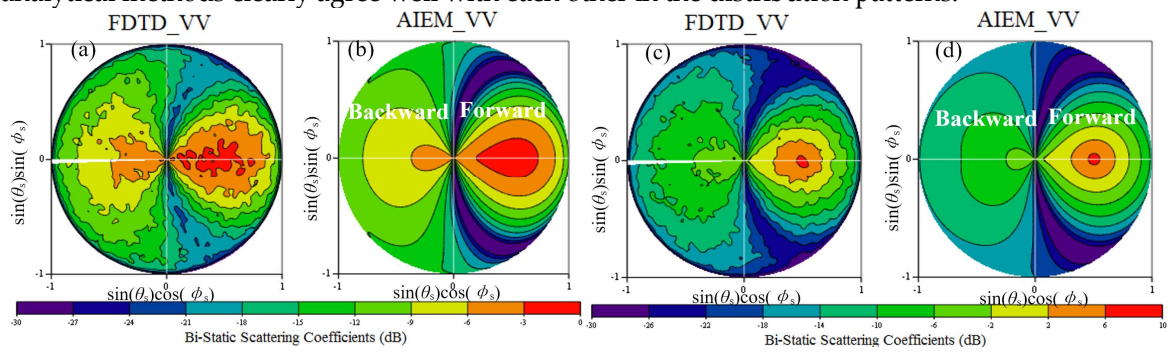

Figure. 6 Comparisons between FDTD simulated upper-space bi-static scattering coefficients (σ_0) and AIEM results, VV, 32 GHz, exponential correlated rough surface, relative permittivity: 6.22-2.86*j*; (a) and (b): correlation length *l*= 48 mm, RMS height *h*= 4 mm; (c) and (d): *l*= 24 mm, *h*= 2 mm.

2.5. The Differences in Experimental and Numerical Studies

Before the results are presented and discussed, there are some differences in the experimental and numerical configurations that should be concluded and noted, for referencing purposes.

First, in the experimental study, the image results are obtained in RCS with unit of m^2; while in the numerical study, the scattering coefficients without unit of m^2, are computed without imaging process. To make a direct correspondence for the speckle results, the PDF of the measured image amplitudes and the simulated scattering amplitudes are normalized by the averaged intensity (RCS σ_{RCS} in experimental images and scattering coefficient σ_0 in numerical simulations), respectively. The averaged σ_{RCS} from the experimental images can also be normalized into σ_0 by using:

$$\sigma_0 = \frac{\sigma_{RCS}}{S_i}, \quad S_i = \rho_{gr}\rho_a \cos(\theta_i) \tag{2}$$

Here ρ_{gr} and ρ_a are the ground range resolution and azimuth resolution, respectively.

In experimental measurement, sufficient measurement samples are gathered by rotating the sample surface in azimuthal direction. In the numerical simulations, a large number of ensemble averages have to be generated.

2.6. Speckle Description

Based on the measured images and the simulated backscattering returns, the speckle properties can be obtained.

First, the probability density function (PDF) can be computed for the amplitude, and compared to the well-known Rayleigh distribution and *K*-distribution. The equations of the two aforementioned PDF models can be found below. The Rayleigh distribution takes the form:

$$p_R(\tilde{A}) = 2\tilde{A} \cdot e^{-\tilde{A}^2}, \tilde{A} \geq 0 \quad \tilde{A} = \frac{A}{< A^2 >} \tag{3}$$

where $\tilde{A}$ is the amplitude normalized by the square root of mean intensity (I=A^2). The *K*-distribution, is given by

$$p_K(\tilde{A}) = \frac{4\alpha^{(\alpha+1)/2}}{\Gamma(\alpha)} \tilde{A}^{\alpha} K_{\alpha-1}(2\sqrt{\alpha}\tilde{A}), \quad \tilde{A} \geq 0 \tag{4}$$

where α is the shape factor coefficients. A larger α will push the *K*-distribution closer to the Rayleigh distribution that describes the fully-developed speckle.

In obtaining the speckle results from experimental and numerical results, first backscattering return amplitudes are normalized by the square root of the mean intensity, which are the concepts of RCS and scattering coefficients, respectively. Then the PDF counting is performed. The α value for the *K*-distribution fitting are obtained by the fourth order moment of $< \tilde{A}^4 >$ (i.e. second order moment of mean normalized intensity), using:

$$< \tilde{A}^4 >= (1 + \frac{1}{\alpha})(1 + \frac{1}{N_{look}}) \tag{5}$$

$$\alpha = 1 \Big/ \left[\left(< \tilde{A}^4 > \Big/ (1 + \frac{1}{N_{look}}) \right) - 1 \right]$$

The standard derivation to mean ratio (γ) of the amplitude can be obtained as:

$$\gamma = \frac{[\mathrm{var}(A)]^{1/2}}{\langle A \rangle} \tag{6}$$

where γ can also be used to check the speckle properties. For reference, the fully developed speckle whose amplitude PDF follows a Rayleigh distribution, is with a theoretical value:

$$\gamma_R = \sqrt{\frac{4}{\pi} - 1} \approx 0.5227 \tag{7}$$

3. Analysis on the Experimental Imaging and Numerical Results

In this section, the imaging results from the rough surface sample, the image amplitude speckle statistics, and the numerical results are to be presented. Then we quote the equivalent scatterer number theory, and knowledge on scattering from sea surfaces, in analyzing the results.

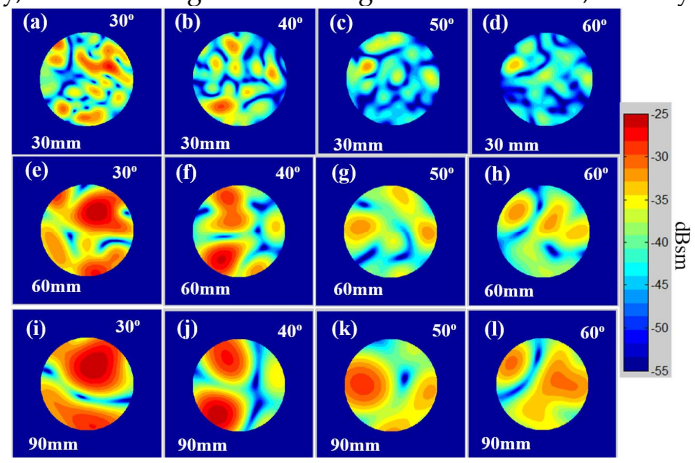

Figure. 7 Image example of the exponential correlated rough surface sample at different resolutions (30mm, 60mm, and 90 mm) and different θ_i (30°, 40°, 50°, and 60°), VV.

3.1. Imaging at different resolutions and incident angles

In Figure. 7, the image examples of the exponential correlated surface are presented at different resolution scales and different values of θ_i. The scattering hot-spots at a VHR scale are observed to

Preprints (www.preprints.org) | NOT PEER-REVIEWED | Posted: 20 July 2018 doi:10.20944/preprints201807.0383.v1

Peer-reviewed version available at Remote Sens. 2018, 10, 1369; doi:10.3390/rs10091369

be fused into those at the lower resolution scales. In addition, clearly, as θ_i increases, the RCS of those spots decrease. These results are measured at one of the 20 ϕ positions, and along with results at other ϕ positions, they are used to produce the speckle results.

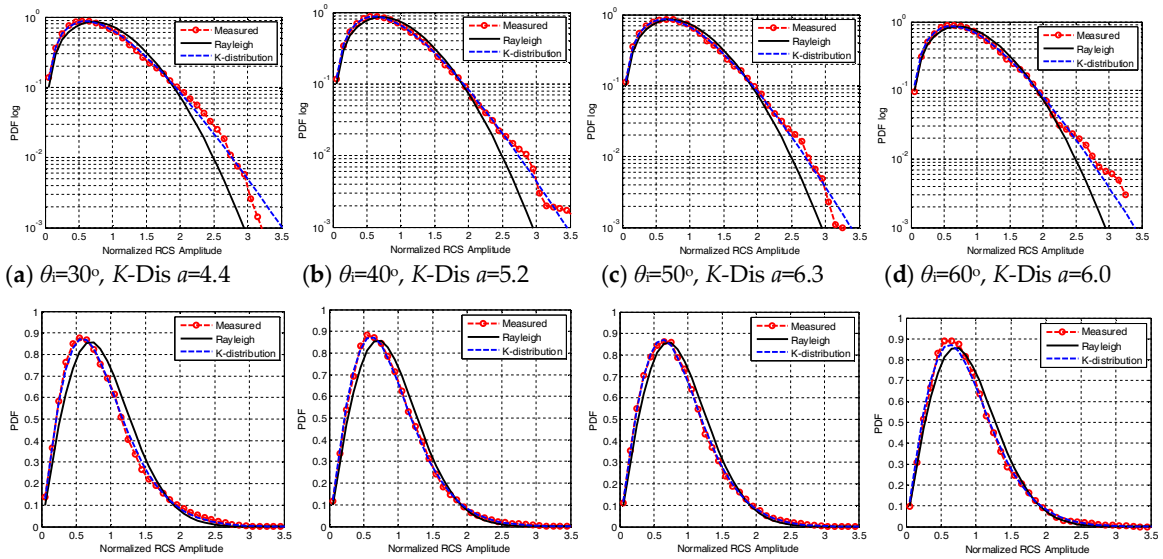

(**a**) θ_i=30°, *K*-Dis α=4.4 (**b**) θ_i=40°, *K*-Dis α=5.2 (**c**) θ_i=50°, *K*-Dis α=6.3 (**d**) θ_i=60°, *K*-Dis α=6.0

Figure. 8 The normalized amplitude PDF curves of measured images at different θ_i, at the resolution cell size of 30 mm, VV, compared with Rayleigh distribution and *K*-distribution. (Sample parameters are shown in Table 1)

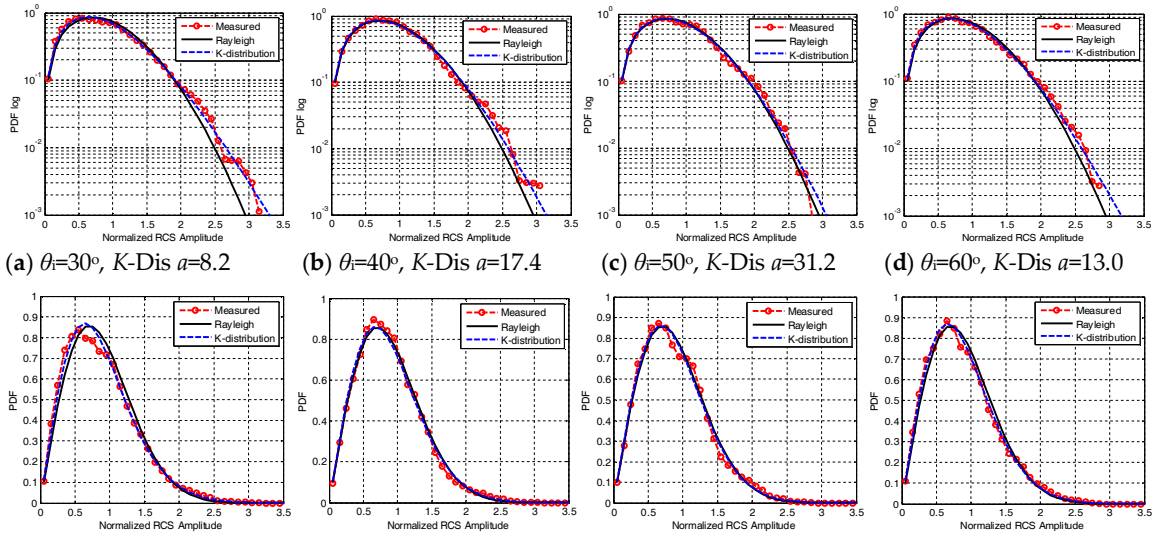

(**a**) θ_i=30°, *K*-Dis α=8.2 (**b**) θ_i=40°, *K*-Dis α=17.4 (**c**) θ_i=50°, *K*-Dis α=31.2 (**d**) θ_i=60°, *K*-Dis α=13.0

Fig. 9 The normalized amplitude PDF curves of measured images at different θ_i, at the resolution cell size of 60 mm, VV, compared with Rayleigh distribution and *K*-distribution. (Sample parameters are shown in Table 1)

In Figure. 8 and Fig. 9, the image amplitude PDFs are plotted and compared to the Rayleigh distribution and the fitted *K*-distribution. In each sub-figure of Figure. 8, the fitted α for the *K*-distribution is marked, where the resolution cell size is set to 30 mm (in azimuth and ground range), or in correlation length, 0.63*l*. Clearly, at the smallest θ_i of 30°, the fitted α is the smallest and the PDF curve is with the tail in semi-log plot most away from the Rayleigh curve. This is also observed in Fig. 9, the results in which are with a resolution cell size of 60mm, or in correlation length, 1.33*l*. Meanwhile, as the resolution cell size enlarges from 30mm to 60mm, the fitted α of *K*-distribution at each θ_i gets larger and the corresponding PDF is more close to the Rayleigh reference. That agrees with common sense. On the other hand, it should be noted that, the PDFs in case of resolution cell size 60mm (Fig. 9) is not fitting the *K*-dis as well as those in the case of

Preprints (www.preprints.org) | NOT PEER-REVIEWED | Posted: 20 July 2018 doi:10.20944/preprints201807.0383.v1

Peer-reviewed version available at Remote Sens. 2018, 10, 1369; doi:10.3390/rs10091369

resolution cell size 30mm (Figure. 8). That is due to the limited size of the sample (250mm in diameter), as it becomes insufficient in providing with rich enough scatter returns.

After the amplitude PDF results based on experimental images are presented, the corresponding averaged RCS σ_{RCS}, the averaged scattering coefficients σ_0, the fitted α of the K-distribution, and the computed γ are listed in the Table4 for referencing purpose. Further, the computed γ in case of different θ_i are plotted via resolution cell sizes in Figure. 10, the coarse but not perfect trends can be well observed, that the γ curves are approaching to the γ_R=0.5227 with the rising of the resolution cell size. The imperfection in those trends is also due to the limited sample size. Also in Figure. 10, the results of computed γ results without antenna pattern compensation conducted in the imaging process are also presented, showing the necessity of such a treatment in the chamber imaging experiments for speckle properties.

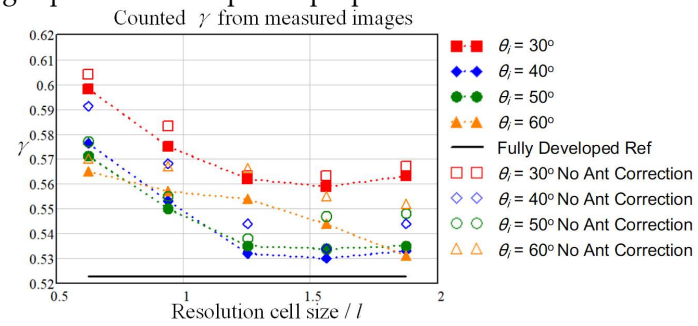

Figure. 10 The computed γ value versus resolution cell size in case of different θ_i from the measured images, VV. "No Ant Correction" denotes for the γ values from images without the antenna pattern correction procedure. (Sample parameters are shown in Table 1)

Table 4. Comparisons of the average intensity values, and amplitude speckle values from the measured images at the resolution cell size of 30mm and 60mm. (Sample parameters shown in Table 1)

Resolution	*θ_i (deg)*	*30*	*40*	*50*	*60*
	AIEM σ_0 (dB)	-6.8	-8.6	-10.4	-11.3
30mm × 30mm	Average σ_{RCS} (dBsm)	-37.5	-39.3	-41.4	-43.9
	Average σ_0 (dB)	-6.4	-7.7	-9.0	-10.5
	a for K-dis	4.5	5.2	6.3	6.0
	Computed γ	0.598	0.576	0.571	0.564
60mm × 60mm	Average σ_{RCS} (dBsm)	-32.0	-33.5	-35.1	-38.8
	Average σ_0 (dB)	-6.9	-7.9	-8.7	-11.4
	a for K-dis	8.2	17.4	31.2	13.0
	Computed γ	0.562	0.532	0.534	0.555

3.2. Results of Numerical Simulations

Next, the numerical results of 1600 realizations are to be presented, the parameters for this set of simulations are concluded in Table 3(set 1). For reference purpose, first, the simulated scattering coefficients over the upper space (bi-static) are presented in Fig. 11, including results by one realization and averaged results by 1600 realizations, in cases of θ_i = 30°, 40°, and 50°. It can be clearly observed that, after averaged over 1600 realizations, the computed bi-static scattering coefficients converges to a smooth distribution.

Preprints (www.preprints.org) | NOT PEER-REVIEWED | Posted: 20 July 2018 doi:10.20944/preprints201807.0383.v1

Peer-reviewed version available at Remote Sens. 2018, 10, 1369; doi:10.3390/rs10091369

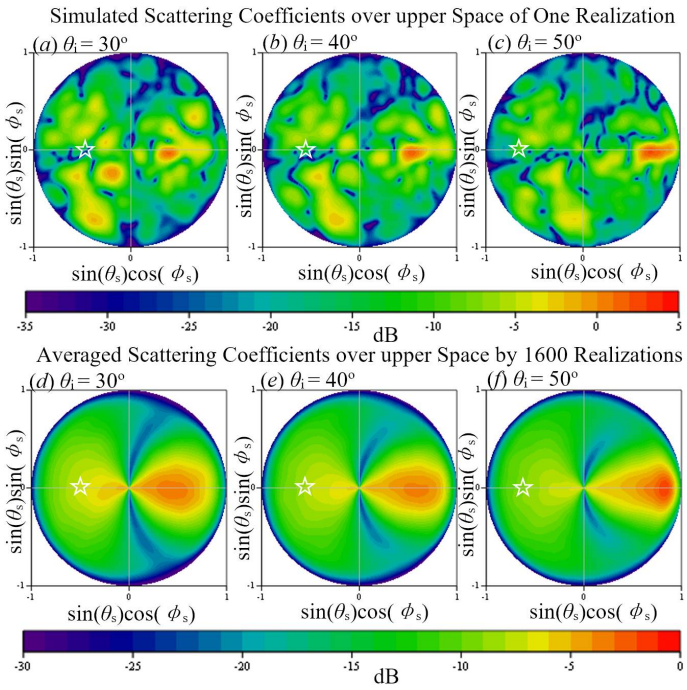

Fig. 11 Results of simulated bi-static scattering coefficients over the upper space, considering different incident angle θ_i. The backscattering angular position is marked by the white-lined star. Sample and computation parameters are in Table 1 and Table 3(set 1).

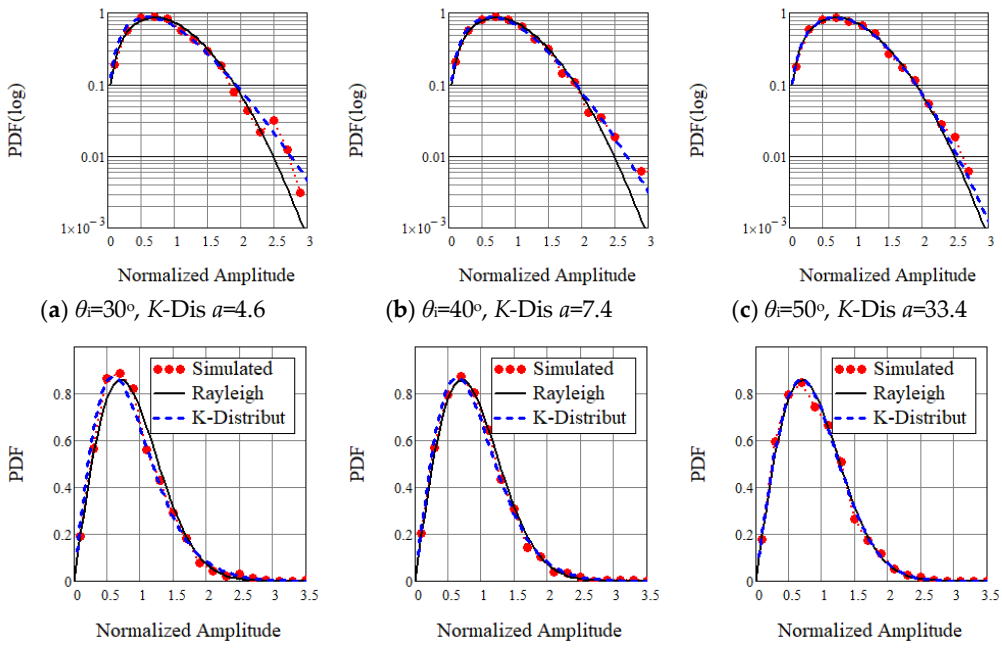

Fig. 12 PDF curves of FDTD-simulated backscattering amplitude at different θ_i, at the footprint size of 30 mm, VV, compared with referencing Rayleigh distribution and *K*-distribution, 1600 realizations. Sample and computation parameters are in Table 1 and Table 3(set 1).

Next the backscattering amplitude PDF results in cases of θ_i = 30°, 40°, and 50°, are compared in Fig. 12, with a 3dB footprint size of 30 mm in diameter. It is very clear that, from θ_i=30° to θ_i=50°, the larger θ_i leads to larger fitted *a*, and the amplitude PDF is more close to the Rayleigh distribution. That trend has also been observed in PDF results from measured images (Figure. 8 and Fig. 9). For reference, the averaged backscattering σ_0, fitted *a* for *K*-distribution, and computed γ are concluded in Table 5. As can be observed from the results in Table 5 and 6, both the experimental imaging and numerical simulation statistics show the same trend, that a larger θ_i (from 30° to 50°) leads to the γ

more close to the fully developed γ_R. That is, as the θ_i get larger in the moderate region, the observed VHR speckle of the exponential correlated sample approaches toward the fully developed speckle.

Table 5. Comparisons of the average intensity values, and amplitude speckle values from simulated backscattering results by 1600 realizations, at the footprint size of 30mm, Sample and computation parameters are in Table 1 and Table 3(set 1).

θ_i (deg)	30	40	50
AIEM σ_0 (dB)	-6.8	-8.6	-10.4
Average σ_0 (dB)	-7.3	-9.0	-10.2
a for K-dis	4.6	7.4	33.4
Computed γ	0.560	0.547	0.531

Table 6. Comparison of amplitude γ in the case of imaging resolution cell/footprint size of 30 mm, at different θ_i, from measured images and simulated backscattering. Sample and computation parameters are in Table 1 and Table 3(set 1).

Method \ θ_i(deg)	30	40	50
Imaging Measurement	0.598	0.576	0.571
Numerical Simulation	0.560	0.547	0.531
Fully Developed Ref	0.5227	0.5227	0.5227

3.3. Equivalent Scatterer Number Prediction

It is well known that the high-resolution speckle properties are different from the fully developed speckle that in the low resolution case. Driven by the trends of high resolution imaging system development and deployment, it becomes increasingly desired to model the high-resolution speckle for land observations. Starting from the low-resolution basis, the amplitude PDF of Rayleigh is built on the condition that many independent scatters contribute to one resolution cell. It is straightforward to explore new speckle descriptions based on the concept of equivalent number of scatterers [5, 12].

In [12], the prediction model for the equivalent number of scatterers per resolution cell was proposed based on the concept of sub-area dividing, to quantitatively predict the speckle properties of rough surfaces in high resolution observations. The objective of [12] wass to provide a quantitative description linking the equivalent number of scatterers N to the well established K-distribution, that a larger N generally leads to speckle more close to Rayleigh and a smaller N leads to a K-distribution further away from the Rayleigh model. A compact formulation is given as in Eq. (8), yielding the equivalent number (N) of distributed scatters within a resolution cell size with respect to surface correlation function types, parameters, incident direction, and observation frequency [12].

$$N = \frac{A_e \,/\, \pi\ell^2}{[-\ln(1-\frac{t}{4k_z^2\sigma^2})]^{2/n}} = N(\frac{A_e}{\pi\ell^2}, k_z\sigma, n) \tag{8}$$

where $k_z = k^*\cos(\theta_i)$, A_e is the area of a resolution cell (not image pixel, and n is 1 for the exponential correlation, 2 for the Gaussian correlation function, with $t = 1$[12].

The experimental results that larger resolution cell size leads to a more Rayleigh distribution, agrees with common sense, as well as the theory prediction for equivalent number of scatterers. In that theory, as the resolution cell size gets larger, the equivalent scatterer number gets larger leading to speckle properties more close to Rayleigh model.

3.4. Similarity to Sea Surface Scattering

In this work, the focus is on the scattering from exponential correlated rough surface,

especially when the resolution is at the level of correlation length. This is a case that will be encountered in the SAR observations of land surface, as the resolution performance keeps evolving. On the other hand, since the correlation length (l) of the sea surface is much larger so that the SAR imaging resolution is already at the level of l, the non-Rayleigh speckle phenomenon in sea speckle has been widely noticed and studied for decades [5, 13, 19-21].

An important description for the non-Rayleigh speckle from sea surface is the two-scale model [13], in which the scattering process from sea surface is viewed as a multiplicative process that, long-scale undulations carry middle or short roughness and both of them are functional for the scattering. That is also an important physical and mathematical description for the K-distribution [13]. Actually one can find the similarity of the scattering process from exponential correlated rough surface to that from sea surface, especially when the resolution cell size is close to the correlation length. In this case, the exponential correlated rough surface contains rich high-frequency roughness leading to scattering source all over the surface as the short-scale scattering (as can be observed in Fig. 13 along the surface interface), meanwhile the undulations at the level of correlation length provide with the relatively long scale carrier for the short scale scattering. The difference in the mechanisms between the scattering from exponential correlated rough surface observed in high resolution, to that from sea surface, is that the lacking of middle scale Bragg scattering, as on exponential correlated surface there isn't the wind driven periodic gurgitation structure.

From both the experimental and numerical results at the very high resolution level, it is interesting that when the incident angle θ_i gets larger from 30° to 50° (moderate region), the speckle are approaching towards the fully developed Rayleigh description. The answer to this phenomena, however, can also be found from the knowledge in scattering mechanisms from sea surface [21-23]. In [23], the *wavelength filtering effect* is concluded for the two-scale or more precisely multi-scale scattering process from sea surface, as that: when the incident angle gets larger from a small value to moderate, the dominating scattering mechanism shifts from long-scale scattering towards short-scale scattering [21-23]. If the effect of long-scale scattering is weaken enough due to the enlarging of θ_i in the moderate region, then the multiplicative process is weaken so that the short-scale scattering that most possibly follows a Rayleigh PDF is taking the dominance of scattering mechanism, as well as the speckle properties. It is interesting that, from the results of simulated sea backscattering in [20], one can find that the speckle results is also approaching toward Rayleigh when θ_i get larger in the moderate region.

Based on the rich knowledge from the research on sea surface scattering, the observed VHR speckle variation from exponential correlated rough surface in the moderate θ_i region, can be clearly explained: the multiplicative effect of scattering process is weaker when the incident angle get larger from small to moderate, as the carrier long-scale scattering gets weaker. Since the short scale scattering acts as the random additive process, in this case, the speckle distribution tends to be the Rayleigh model as the θ_i get larger.

4. Discussion

The widely applied K-distribution in modeling non-Rayleigh scattering speckles, can be either descripted based on the concepts of equivalent number of (independent) scatter N [5,12], and the two-scale scattering of multiplicative process [13]. To further explore the VHR speckle properties from exponential correlated rough surface as a significant description for ground roughness, and to discuss the dominating factors, another set of computations are performed for analysis (parameters in Table 3 set 2). Specifically, different RMS height h are considered: 2mm (0.21λ), 4mm (0.43λ), 8mm (0.85λ), 12mm (1.28λ@32GHz) at θ_i=30°. For each cases of h, still 1600 realizations are computed for the speckle analysis. In Fig. 13, the recorded Electric fields at 32GHz in the incident plane cut of the computation domain in one specific realization were presented, as an intuitive exhibition for the difference of scattering process in case of different h. It seems that, when h=4mm, occasional specular reflection may contribute to the backscattering of θ_i= 30°. That is very possible, as in the scattering coefficient results of Fig. 14, the backscattering at h=4mm is larger than those at

h=2mm, h=8mm, and h=12mm. In Fig. 14, it is also interesting to observe that, as the h changes from 2mm to 12mm, the dominate bi-static scattering region gradually moves from the forward region (h=2mm) to the backward region (h=12mm). Also, the averaged computed scattering coefficients are listed in Table 4, and a good agreement with the AIEM results can be observed.

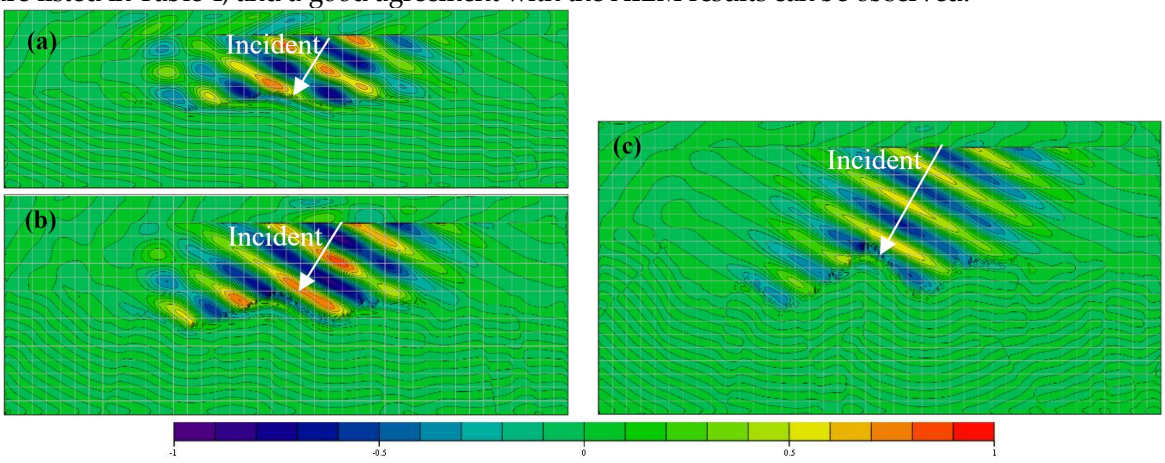

Fig. 13 Recorded total field (E-Field, maximum normalized, real part) in the incident plane cut from the exponential correlated rough surface simulation, θ_i= 30°. (a) h=2mm, (b) h=4mm, (c) h=8mm.

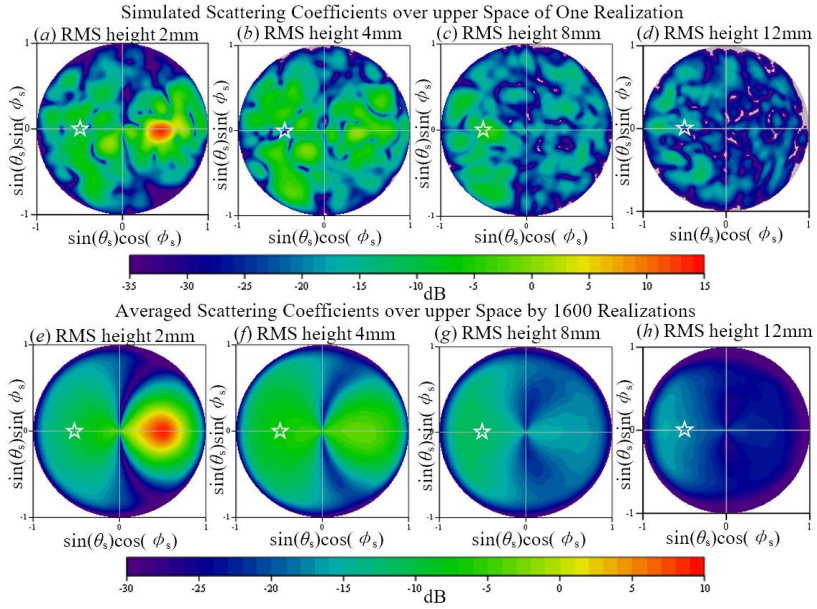

Fig. 14 Results of simulated bi-static scattering coefficients over the upper space, considering different RMS height (h). The backscattering angular position is marked by the white-lined star. Sample and computation parameters are in Table 1 and Table 3(set 2).

The computed amplitude speckle results are then presented in Figure. 15 and Table 4, showing that: at the lowest and highest considered RMS height h values, the backscattering speckle amplitude PDF is very close to the Rayleigh distribution; meanwhile at the moderate h of 4mm, the PDF is away from the Rayleigh one. The observed trends of speckle properties are interesting that it can be directly explained by neither the concept of equivalent number of scatterers, nor the two scale-scattering process. The equivalent number of scatterers theory predict that, the N varies from several, to tens and then to thousands, as the RMS height changes from 2mm to 12mm, at the resolution level of 30mm and θ_i=30°. At the same time, the long scale undulate gets more severe as the RMS height gets larger, the two scale multiplicative scattering process should be strengthened. Clearly, none of the two theory that produces monotonous trend prediction, can be separately used to explain the data results with such a non-monotonous trend.

Actually, it is most possible that both of the two effects should be considered in analyzing and further modeling the VHR speckle from exponential correlated rough surface. When the RMS height is 2mm, the slope of the rough surface is very small (0.042). Although the predicted equivalent number of scatterers within resolution cell size is small, those short-scale scatters remains a random process without notable long-scale modulation. Therefore, with a large number of realizations (or return cells) the speckle remains the fully developed Rayleigh description. When the RMS height is 12mm, the slope of the rough surface gets to 0.25, the process of long scale modulation of short-scale scattering should be notable. However, the equivalent scatterer number is too large (thousands) in this case, it is very likely that such a large amount of scatters overwhelms the modulation effect, so that the VHR speckle is close to the fully developed again. Then it is worthy to get back to the case of h=4mm. One can found that, in this case, the scatterer number is moderate (tens) not large enough, then the notable two-scale modulation effect drives the speckle PDF away from the Rayleigh distribution to the K-distribution with a moderate a.

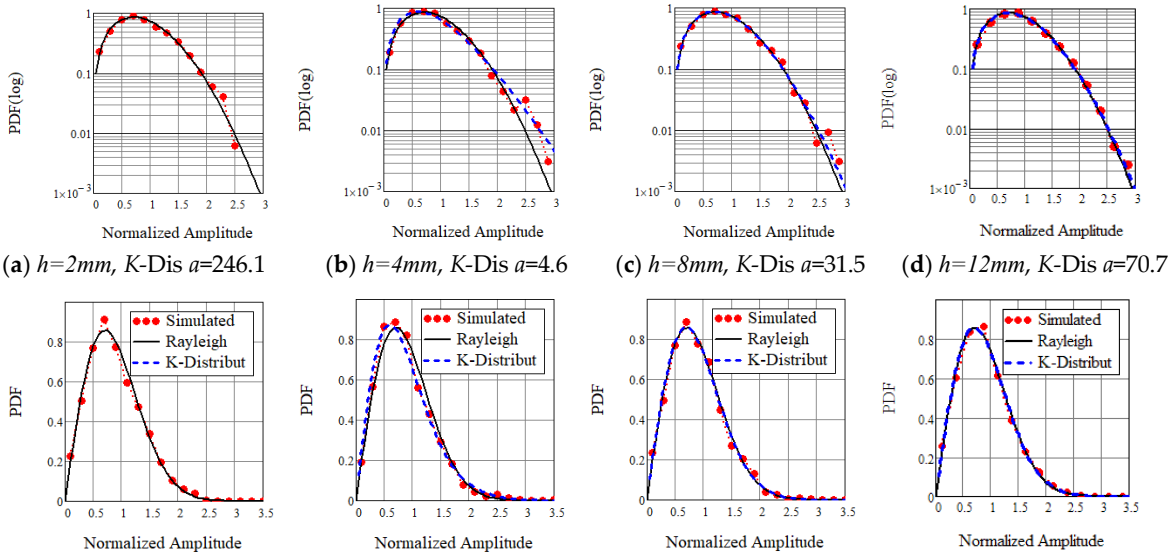

(**a**) h=2mm, K-Dis a=246.1 (**b**) h=4mm, K-Dis a=4.6 (**c**) h=8mm, K-Dis a=31.5 (**d**) h=12mm, K-Dis a=70.7

Figure. 15 PDF curves of FDTD-simulated backscattering amplitude at θ_i=30°, considering exponential correlated surface with different h, (a): h=2mm; (b): h=4mm; (c): h=8mm; (d): h=12mm. VV, compared with referencing Rayleigh distribution and K-distribution, 1600 realizations. Sample and computation parameters are in Table 1 and Table 3(set 2).

Table 7. Comparisons of the average intensity values, and amplitude speckle values from simulated backscattering results by 1600 realizations, at the footprint size of 30mm(3.2λ), Sample and computation parameters are in Table 1 and Table 3(set 2).

RMS height h	*2mm*	*4mm*	*8mm*	*12mm*
AIEM σ_0 (dB)	-10.4	-6.8	-11.8	-18.2
Numerical σ_0 (dB)	-10.0	-7.3	-12.0	-17.7
Amplitude γ	0.525	0.56	0.535	0.528
a for K-dis	246.1	4.6	31.5	70.7
*ENS Prediction N**	2.4	43.4	719.9	3668

*Equivalent number of scatterers is predicted using Eq. (8).

After all, the presented experiments and numerical results in this paper partially support either the equivalent number of scatterers prediction theory or the two-scale model of multiplicative process, and both of them can be found informational and perspective in explaining the numerical results presented in this section. For concluding their application advantages, the equivalent number of scatterers may be very useful in setting a bar for the VHR speckle modeling on exponential correlated rough surfaces, below which the multiplicative scattering process should be considered, and above that bar the Rayleigh model can be sufficient for modeling speckles.

4. Conclusion

In this work, the very high-resolution (VHR) speckle properties from exponential correlated rough surfaces representing ground roughness is investigated by experimental measurements and numerical simulations. Results reveal that in describing VHR speckles, both the concepts of equivalent number of scatterers and scattering scale effects related to the scattering mechanisms are important factors for the exponential correlated rough surface. It is evident from the results that, if the equivalent number of scatterers is not sufficiently large, the two-scale multiplicative scattering process or any other that destroy the independent additive scattering process must be considered in modeling the VHR speckle from exponential correlated rough surface. Also from the numerical simulation, it is found that the dominance by the sufficient large equivalent number of scatterers is also observed, and that leads the VHR speckle properties close to the fully developed model even when the resolution cell size is below the correlation length.

Supplementary Materials: The following are available online at www.mdpi.com/xxx/s1, Figure S1: title, Table S1: title, Video S1: title.

Author Contributions: Conceptualization, Ming Jin and Kun-Shan Chen; Methodology and Writing-Original Draft Preparation, M. Jin; Investigation and Visualization, Dengfeng Xie; Writing-Review & Editing and Funding Acquisition, Prof. Kun-Shan Chen.

Funding: This research was funded by the [National Science Foundation of China] grant number [41531175, 61701496], as well as the [the State Key Laboratory of Remote Sensing Young Researcher Funds] grant number [16RC-03].

Conflicts of Interest: The authors declare no conflict of interest."

References

1. F. T. Ulaby, R. K. Moore, and A. K. Fung, *Microwave remote sensing: active and passive*. Reading, MA, USA: Addison-Wesley, 1981.
2. L. Tsang, J. A. Kong, and K. H. Ding, *Scattering of Electromagnetic waves: Theories and Applications*, NewYork, USA: John Wiley & Sons, 2000.
3. J. S. Lee, E. Pottier, *Polarimetric Radar Imaging: From Basics to Applications*. Boca Raton, FL, USA: CRC Press, 2009.
4. K. S. Chen, L. Tsang, K. L. Chen, T. H. Liao, J. S. Lee, "Polarimetric simulations of SAR at L-Band over bare soil using scattering matrices of random rough surfaces from numerical three-dimensional solutions of Maxwell equations," *IEEE Trans. Geosci. Remote Sens.*, vol. 52, no. 11, pp. 7048-7058, 2014.
5. E. Jakeman and P. N. Pusey, "A model for non-Rayleigh sea echo," *IEEE trans Antennas Propagat.*, vol. AP-24, no. 6, pp. 806-814, 1976.
6. E. Jakeman, "On the Statistics of K-distributed noise," *Journal of Physics A: Mathematical and General*, 13, pp. 31-48, 1980.
7. H. J. Kim, J. T. Johnson, "Radar images of rough surface scattering: comparison of numerical and analytical models," *IEEE Trans. antennas propagat.*, vol. 50, no. 2, pp. 94-100, 2002.
8. A. Nashashibi, F. T. Ulaby, K. Sarabandi, "Measurement and modeling of the millimeter-wave backscatter response of soil surface," *IEEE Trans. on Geosci. Remote Sens.*, vol. 34, no. 2, pp. 561-572, 1996.
9. K. Sarabandi and Y. Oh, "Effect of antenna footprint on the statistics of radar backscattering from random surfaces," *Proc. IEEE IGARSS*, Firenze, Italy, pp.927-929, 1995.
10. S. Allain, L. Ferro-Famil, E. Pottier, and J. Fortuny, "Influence of resolution cell size for surface parameter retrieval from polarimetric SAR data," *Proc. IEEE IGARSS*, Toulouse, France, pp.440-442, 2003.
11. G. Nesti, J. Fortuny and A. J. Sieber, "Comparison of backscattered signal statistics as derived from indoor scatterometric and SAR experiments," *IEEE Trans. Geosci. Remote Sens.*, vol. 34, no. 5, pp. 1074-1083, 1996.
12. G. Di Martino, A. Iodice, D. Riccio, G. Ruello, "Equivalent Number of Scatterers for SAR Speckle Modeling," *IEEE Trans. on Geosci. Remote Sens.*, vol. 52, no. 5, pp. 2555-2564, 2014.
13. K. D. Ward, R. J. A. Tough, and S. Watts, *Sea Clutter: Scattering, the K Distribution and Radar Performance*. London, U.K.: Inst. Eng. Technol., pp. 106-112, 2006.

14. B. Rabus, H. Wehn, and M. Nolan, "The Importance of Soil Moisture and Soil Structure for InSAR Phase and Backscatter, as Determined by FDTD Modeling," *IEEE Trans. on Geosci. Remote Sens.*, vol. 48. no. 5, pp. 2421-2429, 2010.
15. I. Giannakis, A. Giannopoulos, and C. Warren, "A Realistic FDTD Numerical Modeling Framework of Ground Penetrating Radar for Landmine Detection," *IEEE J. Selected Topics in Appl. Earth Observation. Remote Sens.*, vol. 9, no. 1, pp. 37-51, 2016
16. M. Bai, M. Jin, N. Ou, and J. Miao, "On Scattering From an Array of Absorptive Material Coated Cones by the PWS Approach," *IEEE Trans. on Antennas Propagat.*, vol. 61, no. 6, pp. 3216-3224, 2013
17. K. S. Chen, T. D. Wu, L. Tsang, Qin Li, J. C. Shi, A. K. Fung, "Emission of Rough Surfaces Calculated by the Integral Equation Method With Comparison to Three-Dimensional Moment Method Simulations," *IEEE Trans. on Geosci. Remote Sens.*, vol. 41. no. 1, pp. 90-101, 2003.
18. A. K. Fung, K. S. Chen, "An update on the IEM surface backscattering model," *IEEE Geosci. Remote Sens. Lett.*, vol. 1, no. 2, pp. 75-77, 2004.
19. F. Nouguier, C.-A. Guérin, and B. Chapron, "Scattering from nonlinear gravity waves: the 'Choppy Wave' model," *IEEE Trans. Geosci. Remote Sens.*, vol.48, no. 12, pp. 4184-4192, 2010.
20. N. Pinel, B. Chapron, C. Bourlier, N. de Beaucoudrey, R. Garello, and A. Ghaleb, "Statistical analysis of real aperture radar field backscattered from sea surfaces under moderate winds by Monte Carlo simulations," *IEEE Trans. Geosci. Remote Sens.*, vol.52, no. 10, pp. 6459-6470, 2014.
21. S. L. Durden, J. F. Vesecky., A physical radar cross-section model for a wind-driven sea with swell. *IEEE Journal of Oceanic Engineering*, 1985, vol. 10, no. 4, pp. 445-451, 1985.
22. S L. Durden, J F. Vesecky., A numerical study of the separation wavenumber in the two-scale scattering approximation (ocean surface radar backscatter). *IEEE transactions on geoscience and remote sensing*, vol. 28, no.2, pp. 271-272, 1990.
23. Fung A K. Backscattering from Multiscale Rough Surfaces with Application to Wind Scatterometry[M]. A rtech House, pp.3-4, 29-42, 2015.